Solar cell with double quantum dot structure

Suha Hadi and Amin Habbeb Al-Khursan

Nassiriya Nanotechnology Research Laboratory (NNRL), Science College, Thi-Qar University, Nassiriya, Iraq

Abstract:

In this work, a double quantum dot (QD) structure is introduced as an intermediate band for high-performance solar cells (SCs). Coupling the dynamical (density matrix) equations with the continuity-current equation and solving them numerically to obtain the quantum efficiency (QE). which allowed to address the interaction between all the states and band of SC which is not possible elsewhere and better than the rate equation modeling. Throughout this modeling, the momentum matrix elements of QD-QD, QD-wetting layer (WL), and WL-barrier transitions are calculated and the orthogonalized plane wave is assumed for WL-QD transitions. Results are simulated both the excitonic and non-excitonic (electron-hole eh) cases and exhibit the importance of adding the QD layer.

The valence band (VB) DQD states have similar occupations while the conduction band (CB) is not. The WL occupations are the smallest in both CB and VB as it works like a reservoir. These results confirm both the importance of adding the intermediate band (QD layer) and the carrier scenarios. The band-to-band recombination rates in the DQD structure are modulated with the energy difference. The VB relaxation rates between states are of the same order and lower than the corresponding CB rates related to their occupation. The occupations in the excitonic model do not much differ from the eh model. A few increments in the excitonic model in the CB and VB barrier-WL relaxation while a reduction in the VB WL-QD and QD-QD relaxation appears. The band-to-band recombination rates in the excitonic model are reduced compared to the eh model. The photo-generation rates have the highest rate at QDs. The quantum efficiency (QE) in the eh model is increased at semi-linear relation with VB relaxation rates while it is increased exponentially with CB rates. Longer relaxation times for WL-QD check it pleas transitions are attained with a wider energy difference. For the DQD structure, the longer relaxations and band-to-band recombinations are accessed depending on the wider energy difference.

Keywords: double quantum dot solar cell, electron-hole model, excitonic model, recombination rate, band-to-band, quantum efficiency.

1-Introduction:

Renewable energy gets more attention, especially solar cells (SCs) that are based on semiconductors with gain power conversion efficiency on the order of 44% [1]. While the conversion efficiency is increased with the multi-junctions, its manufacture becomes complex due to its heterogeneous with accumulating internal losses. Triple-junction lattice-matched semiconductor SCs explan in differol manaor. This efficiency can be increased to more than 60% by realizing the intermediate band solar cell (IBSC) with triple-band absorption by only a single junction. This is due to incorporating

the completely quantized quantum dot (QD) nanostructures [1, 2]. IBSC can expand the photo-sensitivity spectrum to longer wavelength response by incorporating the QDs [3]. The intermediate band (IB) is a material that has levels inserted into a semiconductor forbidden bandgap. An electron-hole (eh) pair from conduction (CB) and valence bands (VB) can be released by two sub-bandgap photons. In this case, a single-junction solar cell empirically simulates the triple-junction solar cells with high efficiency [4].

III-V QD solar cells (QDSCs) suffer from the thermal coupling between IB and CB. This thermal coupling process excites carriers between them and deletes the two-photon absorption, and then reducing the bandgap energy [5]. The second problem is the band alignment of Type-I InAs/GaAs. These two problems, strengthen the radiative recombination, i.e. shortening the lifetime which removes the need for the two-photon excitation, and the open-circuit voltage is lowered then, and a prolonged carrier lifetime is required. Thus, D. Kim et al. are proposing InAs/GaAsSb type-II QD structure for long-life carriers [6]. Ramiro et al. use the AlGaAs barrier layer with the wide bandgap InAs/InGaP QD structure to reduce thermal escape. The enlarged bandgap is shown to be efficient in reducing both inter-and intra-band gap relaxations from QDs [7]. High photon absorption requires an IB with empty states (QD valence subbands) for receiving electrons from the VB and states filled with electrons (QD conduction subbands) to excite electrons to the CB [5]. D. Kim et al. study the partial filling of the IB by using Si dopants to the QDs with AlAs as a cap layer to reduce Si doping density to achieve the required filling where a QD carrier lifetime enhancement is justified [5]. Then, D. Kim et al. studied InAs-QD/GaAsSb-quantum well hybrid system with GaAs as an interlayer [8]. A set of theoretical works on QDSCs by exploiting kinetics of QD with a drift-diffusion formula is presented. The QD thermal spreading of holes gives the maximum achievable harvesting of QDSCs [9]. A model exploits experimental parameters of photo-generation and carrier dynamics by detailing the thermally-assisted carrier processes [10-12].

Progress in the growth technology makes growing QDs with different shapes and sizes is an attainable task. So, double QD (DQD) is proposed to develop the linear and nonlinear response of QD structures due to the possibility of manipulation between states [13, 14] and the Y-configuration DQD system is then introduced [15]. The wetting layer (WL) effect cannot be avoided, therefore orthogonalized plane wave (OPW) between QD states and WL is taken into account for more reality of formulation [16]. The work with the DQD structure exhibits the best linear and nonlinear optical properties [17, 18].

Since DQD contains two QDs with different sizes, see Fig. 1, extra manipulation with short and/or long relaxation rates and momentum matrix elements of high and/or weak strengths is exhibited. This can be used to treat the shortcomings in the QDSC and obtain high performance. This work begins from the calculation of energy subbands of the DQD system and then momentum matrix elements between states and/or bands are calculated since we consider the barrier, WL, and QD regions in the formulation. The dynamic description of the transitions in the QDs (i.e. QD-QD), WL-QD, and barrier-WL is done by using the density matrix theory (DMT) where two types of transitions are considered: relaxation from/to the respective states (R) and the band-to-band transition rates (U). This type of formulation is used for the first time and different from that in [10, 19] where the rate equations are connected with the continuity-current equation. The DMT considers the interaction between all states by using the density operator (ρ_{ij}) between states i and j that are either respective or not, which is not taken elsewhere. The analytical derivation to obtain the current density of layers of the solar cell structure which is performed by [20, 21] (see Fig. 2). It is then used in the continuity-current equation which is connected with the DMT to obtain DQDSC characteristics. This work deals with two types of modeling: The electron-hole (eh) model where different relaxation times from the electron and hole states are considered. The second model is the exciton model where the same electron and hole relaxation times are taken. Need to cite refference.

1.InAs DQD structure:

The DQD structure used in the SC structure is composed of two QDs. The shape of each QD is an InAs quantum disk of radius *an* and height *h*. The size of the first QD is (*h*= 2 nm, *a* =14 nm) while that of the second QD is (*h*=3.5 nm, *a* =13 nm). Taking the ground state (GS) of each QD in the conduction and

valence bands (CB and VB) results in 4 subbands $|0\rangle, |1\rangle, |2\rangle,$ and $|3\rangle$. Only a single state for each band in the WL is considered ($|4\rangle$ and $|5\rangle$). Additionally, the CB and VB of the barrier are considered. The energy band diagram of the DQDSC structure is shown in Fig. 1.

3. Derivation of QE in solar cell:

The minority carrier-continuity equations for holes in the n-side and electrons in the p-side, respectively, are written as [12, 13].

$$-\frac{1}{q}\frac{\partial J_p}{\partial x} - \frac{\delta p_n}{\tau_p} + G_p = \frac{\partial p_n}{\partial t} \qquad (1)$$

$$\frac{1}{q}\frac{\partial J_n}{\partial x} - \frac{\delta n_p}{\tau_n} + G_n = \frac{\partial n_p}{\partial t} \qquad (2)$$

where the excess hole (electron) concentration due to external excitations is expressed as $\delta p_n = p_n - p_{n0}$, ($\delta n_p = n_p - n_{p0}$), with $p_n (n_p)$ is the total hole (electron) concentration in the n-region (p-region), and $p_{n0}(n_{p0})$ is the hole (electron) concentration without any injection. τ_p and τ_n are the hole and electron lifetimes, respectively. $J_p (J_n)$ is the photocurrent density of holes (electrons) in the n (p) region? The distance-dependent generation rate of the electron-hole pair $G_p (G_n)$ is the photon generation rate in the p-(n-) region at a steady state. The following definitions of the generation rate depending on the region:

$$G_{n\ell} = (1-R)\alpha_{n\ell}\Phi\exp\left\{-\left(\alpha_{n\ell}x_j + \alpha_d W + \alpha_{p\ell}\left[x - x_j - W\right]\right)\right\} \qquad (3)$$

$$G_{p\ell} = (1-R)\alpha_{p\ell}\Phi\exp\left\{-\left(\alpha_{p\ell}x_j\right)\right\} \qquad (4)$$

where the distance (x) dependent absorption coefficient is $\alpha_{p\ell}$, $\alpha_{n\ell}$, $\alpha_{d\ell}$ are the absorption coefficients of the $p-$, $n-$, and depletion layers, respectively, $\ell(=QD, w, B)$ refers to the layers: QD, WL, or barrier, x_j is the junction depth, and W is the depletion width, see Fig. 2, the air-semiconductor optical reflectivity factor is R and Φ is the illuminated photon number. Since the diffusion process is the dominant one for the minority current density, then one can put [13].

$$\frac{-1}{q}\frac{\partial J_p}{\partial x} \square D_p \frac{\partial^2 \delta p_n}{\partial x^2} \qquad (5)$$

$$\frac{1}{q}\frac{\partial J_n}{\partial x} \square D_n \frac{\partial^2 \delta n_p}{\partial x^2} \qquad (6)$$

Note that D_p and D_n are the diffusion coefficients for the hole and electron. Using Eqs. (5) and (6) into Eqs. (1) and (2) which are analytically solved to obtain the relations of the carrier density in the regions. Note that the solution is regarding the QD region only since the main contribution to the generation rate is coming from the QD layer due to its high absorption compared with WL and barrier. After some manipulations, the relation of the hole density is derived. It is given by [12].

$$\delta p_n = \frac{\alpha_n \phi(1-R)\tau_p}{\left(\alpha_n^2 L_p^2 - 1\right)}\left\{\frac{\cosh(x/L_p)}{\sinh(x_j/L_p)}\left[e^{-\alpha_n x_j} - \frac{(D_p\alpha_n^2 - S_p)}{([D_p/L_p^2] - S_p)}e^{(x_j/L_p)}\right]\right.$$

$$\left. + \frac{(D_p\alpha_n^2 - S_p)}{([D_p/L_p^2] - S_p)}e^{(x/L_p)} - e^{-\alpha_n x}\right\} \qquad (7)$$

In the above relation; S_p refers to the surface recombination velocity of holes. $L_p(=\sqrt{\tau_p D_p})$ is the hole diffusion length? Similarly, the p-region electron density is derived. It is given by [12].

$$\delta n_p = \frac{\alpha_p \phi (1-R) \tau_n}{(\alpha_p^2 L_n^2 - 1)} e^{-(\alpha_n x_j - \alpha_d W)} \{ e^{-(x-x_j-W/L_n)}$$

$$+ \frac{\sinh(x-x_j-W/L_n)}{\sinh(H'/L_n)[\frac{D_n}{L_n^2}-S_n]} [(\alpha_p^2 - S_n)e^{-\alpha_p H'}]$$

$$-[\frac{D_n}{L_n^2}-S_n]e^{-H'/L_n} - e^{-\alpha_p(x-x_j-W)} \} \tag{8}$$

where $H' = H - x_j - W$, see Fig. 2. S_n is the surface recombination velocity of electrons? $L_n (=\sqrt{\tau_n D_n})$ is the electron diffusion length? The photocurrent density of holes in the n-region is $J_p \approx -qD_p \frac{\partial}{\partial x} \delta p_n$ and that of electrons in the p-region is $J_n \approx -qD_n \frac{\partial}{\partial x} \delta n_p$. The drift photocurrent density from the depletion region is defined by [13].

$$J_{dr} = q\phi(1-R)e^{-\alpha_n x_j}\left(1-e^{-\alpha_d W}\right) \tag{9}$$

while the QE is defined by the relation [13]

$$QE = \frac{(J_p + J_n + J_{dr})}{q\phi(1-R)} \tag{10}$$

4.The dynamical equations of the DQD system:

The DQD system Hamiltonian is given by,

$$H = H_0 + H_{int} + H_{relax} \tag{11}$$

where H_0 is the unperturbed Hamiltonian, H_{int} is the interaction Hamiltonian while H_{relax} is for relaxations. The unperturbed Hamiltonian is given by

$$H_0 = \sum_{j=0}^{7} \hbar w_j |j\rangle\langle j| \tag{12}$$

with $\hbar w_j$ is the jth state energy. The interaction Hamiltonian is given by

$$H_{int} = \begin{bmatrix} 0 & -\hbar\beta_{01} & -\hbar\beta_{02} & -\hbar\beta_{03} & -\hbar\beta_{04} & 0 & 0 & 0 \\ -\hbar\beta_{01} & a_{10} & -\hbar\beta_{12} & -\hbar\beta_{13} & -\hbar\beta_{14} & 0 & 0 & 0 \\ -\hbar\beta_{20} & -\hbar\beta_{21} & a_{20} & -\hbar\beta_{23} & 0 & -\hbar\beta_{25} & 0 & 0 \\ -\hbar\beta_{30} & -\hbar\beta_{31} & -\hbar\beta_{32} & a_{30} & -\hbar\beta_{35} & 0 & 0 & 0 \\ -\hbar\beta_{40} & -\hbar\beta_{41} & 0 & 0 & a_{40} & -\hbar\beta_{45} & -\hbar\beta_{46} & 0 \\ 0 & 0 & -\hbar\beta_{52} & -\hbar\beta_{53} & -\hbar\beta_{54} & 0 & a_{56} & -\hbar\beta_{57} \\ 0 & 0 & 0 & 0 & -\hbar\beta_{64} & 0 & 0 & -\hbar\beta_{67} \\ 0 & 0 & 0 & 0 & 0 & -\hbar\beta_{75} & -\hbar\beta_{76} & 0 \end{bmatrix} \tag{13}$$

Note that $\beta_{ij} = \dfrac{a_{ij}}{2} + \dfrac{1}{T_2}$ with a_{ij} is the Einstein coefficient ($a_{ij} = \mu_{ij}^2 \omega_{ij}^2 / 3\pi\hbar\varepsilon_0 c^3$) and T_2 is the dephasing time [14]. Under the density matrix equation

$$\frac{d\rho}{dt} = -\frac{i}{\hbar}[H,\rho] \tag{14}$$

By using the DQD system Hamiltonian, Eq. 12, under the rotating wave approximation, the dynamical approach for DQD system is written as

$$\rho_{00}^{\square} = -\gamma_{10}\rho_{00} - \gamma_{04}\rho_{00} + \gamma_{40}\rho_{44} + \gamma_{10}\rho_{11} + \beta_{01}(\rho_{10}-\rho_{01}) + \beta_{02}(\rho_{20}-\rho_{02})$$
$$+ \beta_{03}(\rho_{30}-\rho_{03}) + \beta_{04}(\rho_{40}-\rho_{04}) + G_{n_{QD}} - (U_{02}+U_{03}).$$

$$\rho_{11}^{\square} = -\gamma_{10}\rho_{11} - \gamma_{14}\rho_{11} + \gamma_{11}\rho_{00} + \gamma_{41}\rho_{44} + \beta_{10}(\rho_{01}-\rho_{10}) + \beta_{12}(\rho_{21}-\rho_{12})$$
$$+ \beta_{13}(\rho_{31}-\rho_{13}) + \beta_{14}(\rho_{41}-\rho_{14}) + G_{n_{QD}} - (U_{12}+U_{13}).$$

$$\rho_{22}^{\square} = -\gamma_{23}\rho_{22} - \gamma_{25}\rho_{22} + \gamma_{32}\rho_{33} + \gamma_{52}\rho_{55} + \gamma_{72}\rho_{77} - \gamma_{27}\rho_{22} + \beta_{20}(\rho_{02}-\rho_{20}) + \beta_{21}(\rho_{12}-\rho_{21})$$
$$+ \beta_{23}(\rho_{32}-\rho_{23}) + \beta_{25}(\rho_{52}-\rho_{25}) + G_{P_{QD}} - (U_{02}+U_{12}).$$

$$\rho_{33}^{\square} = -\gamma_{32}\rho_{33} - \gamma_{35}\rho_{33} + \gamma_{23}\rho_{22} + \gamma_{53}\rho_{55} + \gamma_{73}\rho_{77} - \gamma_{37}\rho_{33} + \beta_{30}(\rho_{03}-\rho_{30}) + \beta_{31}(\rho_{13}-\rho_{31})$$
$$+ \beta_{32}(\rho_{23}-\rho_{32}) + \beta_{35}(\rho_{53}-\rho_{35}) + G_{P_{QD}} - (U_{03}+U_{13}).$$

$$\rho_{44}^{\square} = -\gamma_{40}\rho_{44} - \gamma_{41}\rho_{44} - \gamma_{46}\rho_{44} + \gamma_{04}\rho_{00} + \gamma_{14}\rho_{11} + \gamma_{64}\rho_{66} + \beta_{40}(\rho_{04}-\rho_{40}) + \beta_{41}(\rho_{14}-\rho_{41})$$
$$+ \beta_{45}(\rho_{54}-\rho_{45}) + \beta_{46}(\rho_{64}-\rho_{46}) + G_{n_w} - U_{45}$$

$$\rho_{55}^{\square} = -\gamma_{57}\rho_{55} - \gamma_{52}\rho_{55} - \gamma_{53}\rho_{55} + \gamma_{25}\rho_{22} + \gamma_{35}\rho_{33} + \gamma_{75}\rho_{77} + \beta_{52}(\rho_{25}-\rho_{52}) + \beta_{53}(\rho_{35}-\rho_{53})$$
$$+ \beta_{54}(\rho_{45}-\rho_{54}) + \beta_{57}(\rho_{75}-\rho_{57}) + G_{P_w} - U_{45}.$$

$$\rho_{66}^{\square} = \frac{A}{q}\left(\frac{dJ_n}{dt}\right) - \gamma_{64}\rho_{66} + \gamma_{46}\rho_{44} + \beta_{64}(\rho_{46}-\rho_{64}) + \beta_{67}(\rho_{76}-\rho_{67}) + AG_{n_B} - U_{67}.$$

$$\rho_{77}^{\square} = -\frac{A}{q}\left(\frac{dJ_p}{dt}\right) - \gamma_{75}\rho_{77} + \gamma_{57}\rho_{55} + \beta_{75}(\rho_{57}-\rho_{75}) + \beta_{76}(\rho_{67}-\rho_{76}) + AG_{P_B} - U_{67}.$$

$$\rho_{10}^{\square} = -\rho_{11}(1-\rho_{00})\tau_{o10}^{-1} - \Delta_{10}\rho_{10} + a_{10}\rho_{00} + \beta_{12}\rho_{20} + \beta_{13}\rho_{30} + \beta_{14}\rho_{40} - \rho_{11}a_{10}$$
$$+ \rho_{12}\beta_{20} + \rho_{13}\beta_{30} + \rho_{14}\beta_{40}.$$

$$\rho_{20}^{\square} = -\rho_{22}(1-\rho_{00})\tau_{o20}^{-1} - \Delta_{20}\rho_{20} + a_{20}\rho_{00} + \beta_{21}\rho_{10} + \beta_{23}\rho_{30} + \beta_{25}\rho_{52} - \beta_{10}\rho_{21}$$
$$+ a_{20}\rho_{22} + \beta_{30}\rho_{23} + \beta_{52}\rho_{25}.$$

$$\rho_{30}^{\square} = -(1-\rho_{00})\tau_{o30}^{-1}\rho_{33} - \Delta_{30}\rho_{30} + a_{30}\rho_{00} + \beta_{31}\rho_{10} + \beta_{32}\rho_{20} + \beta_{10}\rho_{31} - \beta_{20}\rho_{32}$$
$$+ a_{30}\rho_{33}.$$

$$\rho_{40}^{\square} = -(1-\rho_{00})\tau_{o40}^{-1}\rho_{44} - \Delta_{40}\rho_{40} + a_{40}\rho_{00} + \beta_{41}\rho_{10} + \beta_{10}\rho_{41} + a_{40}\rho_{44}.$$

$$\rho_{21}^{\square} = -(1-\rho_{11})\tau_{o21}^{-1}\rho_{22} - \Delta_{21}\rho_{21} + \beta_{20}\rho_{01} + a_{21}\rho_{11} + \beta_{23}\rho_{31} - \beta_{10}\rho_{20} + \beta_{31}\rho_{23} + a_{21}\rho_{22}.$$

$$\rho_{23}^{\square} = -(1-\rho_{33})\tau_{o23}^{-1}\rho_{22} - \Delta_{23}\rho_{23} + a_{23}\rho_{33} + \beta_{25}\rho_{53} + a_{23}\rho_{22} + \beta_{53}\rho_{25}.$$

$$\rho_{25}^{\square} = -(1-\rho_{55})\tau_{o25}^{-1}\rho_{22} - \Delta_{25}\rho_{25} + b_{23}\rho_{35} + a_{25}\rho_{55} - \beta_{35}\rho_{23} - \beta_{25}\rho_{23}.$$

$$\rho_{31}^{\square} = -(1-\rho_{11})\tau_{o31}^{-1}\rho_{33} - \Delta_{31}\rho_{31} + \beta_{30}\rho_{01} + a_{31}\rho_{11} + \beta_{32}\rho_{21} - \beta_{01}\rho_{30} + \beta_{21}\rho_{32} + a_{31}\rho_{33}.$$

$$\rho_{35}^{\square} = -(1-\rho_{55})\tau_{o35}^{-1}\rho_{33} - \Delta_{35}\rho_{35} + \beta_{32}\rho_{25} + a_{35}\rho_{55} - \beta_{25}\rho_{32}.$$

$$\rho_{41}^{\square} = -(1-\rho_{11})\tau_{o41}^{-1}\rho_{44} - \Delta_{41}\rho_{41} + \beta_{40}\rho_{01} + a_{41}\rho_{11} - \beta_{01}\rho_{40} + a_{41}\rho_{44}.$$

$$\rho_{46}^{\square} = -\tau_{o46}^{-1}(1-\rho_{66})\rho_{44} + a_{46}\rho_{66}.$$

$$\rho_{57}^{\square} = -(1-\rho_{77})\tau_{o57}^{-1}\rho_{55} + a_{56}\rho_{77}.$$

$$\rho_{45}^{\square} = -(1-\rho_{55})\tau_{o45}^{-1}\rho_{44} + a_{45}\rho_{55}.$$

$$\rho_{67}^{\square} = -(1-\rho_{77})\tau_{o67}^{-1}\rho_{66} + a_{67}\rho_{77} \qquad (15)$$

The diagonal relaxation γ_{jj} is the state $|j\rangle$ relaxation, while γ_{ij} are referring to those between states. $G_{n(p)_\ell}$ refers to the n(p) layer photo-generation rate of QD (WL, barrier) layers, $\ell(=QD, \text{w}, B)$, that are defined in Eqs. (3) and (4). $n_{InAs}(n_{GaAs})$ is the intrinsic carrier concentration in the InAs QD (GaAs barrier), they are normalized to a geometrical factor $(\dfrac{h_{QD}}{N_Q}r_B)$ to attain the intrinsic occupation. Note that N_Q, h_{QD}, r_B are the QD density, QD height, and density of states (DOS) in the barrier. A is the area of the barrier layer, q is the electronic charge, and $\dfrac{dJ_p}{dt}(\dfrac{dJ_n}{dt})$ refers to the time derivative of the hole (electron) current density. $\tau_{r_o}(\tau_{r_w})$ is the QD (WL) relaxation rate and τ_{r_w} is also considered for the 3-D barrier layer. The times $\tau_{0_{ij}}$ are the recombination times between states i and j. Finally, Δ_{ij} is the frequency difference between states i and j.

5.Recombination rates:

The recombination rates for band-to-band transitions between DQD states are defined as

$$U_{ij} = (\frac{1}{\tau_{r_o}})(\rho_{ii}\rho_{jj} - n_s^2) \qquad (16)$$

With $n_s = n_{InAs}\dfrac{h_{QD}}{N_Q}$ and i refers to the CB QD states $(i=0,1)$ and j is refer to the VB QD states $(j=2,3)$. For WL and barrier, band-to-band, transitions they are defined by

$$U_{\ell m} = (\frac{1}{\tau_{rw}})(\rho_{\ell\ell}\rho_{mm} - n_G^2) \qquad (17)$$

Note that ℓ refers to the CB WL (barrier) $\ell=4\,(6)$ and $m=5(7)$ to the VB WL (barrier). Then, $n_G = \dfrac{n_{GaAs}}{\rho_B}$, while the effective barrier DOS is [22]

$$\rho_B = 2[\frac{2m_o\pi k_\beta T}{\hbar^2}]^{(3/2)} \qquad (18)$$

The relaxation rate between respective states (or bands) is defined as

$$R_{ij} = \rho_{ii}(1-\rho_{jj})(\frac{1}{\tau_{0ij}}) \qquad (19)$$

6.Relaxation rates under Fermi distribution:

The DQDSC system is relaxed into quasi-thermal equilibrium by going through the Fermi distribution of carriers in their states. Tables 1 and 2 are lists the structure parameters and the absorption of layers. The relaxation rates, such as R_{57}, R_{35}, R_{23}, R_{46}, R_{41}, R_{10} are taken from Table 3. These are the capture rates, their escapes such as R_{75}, R_{01} are taken after considering their Fermi equilibria and are listed below. Since both barrier, WL, and QD states are considered in this work, the Fermi equilibrium between relaxation times is considered as follows

$$\tau_{o_{d_i w_\sigma}} = \tau_{o_{w_\sigma d_i}} \frac{2N_Q}{r_{WL}} \exp\frac{\Delta E_{d_i w_\sigma}}{k_\beta T} \qquad (19)$$

$$\tau_{o_{d_i d_j}} = \tau_{o_{d_j d_i}} \exp \frac{\Delta E_{d_i d_j}}{k_\beta T} \tag{20}$$

$$\tau_{o_{W_\sigma B_\sigma}} = \tau_{o_{B_\sigma W_\sigma}} \frac{\rho_{WL}}{\rho_B z_{WL}} \exp \frac{\Delta E_{W_\sigma B_\sigma}}{k_\beta T} \tag{21}$$

Note that the relaxations are normalized through the effective density of states (DOS) of WL ρ_{WL}, given by [22]

$$\rho_{WL} = [\frac{m_o k_\beta T}{\pi \hbar^2}]^{(3/2)} \tag{22}$$

7.Results and discussion:
7-1Relaxation rates:
a-eh model at Fermi equilibrium:

Fig. 3 shows the time series of occupation probability of DQD states in addition to the WL and the barrier layer. The highest occupations are shown in the barrier layer in the CB and VB $(\vert 6 \rangle, \vert 7 \rangle)$, as it is taken in the initial conditions where the barrier is assumed to be fully occupied, initially. Mainly, the occupations are declining exponentially except CB QDs (ρ_{00}, ρ_{11}). The VB occupations are emptied after ~0.7ns which refers to electron accommodation by both injection and relaxations. The WL is taken as a single state, which is a common assumption in the literature [23, 24]. Fig. 3 shows the raise of WL occupation from zero in both CB and VB, then VB occupation in the WL ρ_{55} goes to near-empty. Our results simulate the expected carrier dynamics between layers (and states). For QD states, the VB DQD states ρ_{22} and ρ_{33} have similar occupations. A high CB occupation for the left QD ρ_{00} compared to that of the right one ρ_{11}. This is acceptable since ρ_{00} is for the CB GS of the DQD system while ρ_{11} is that of ES.

Fig. 4 shows the carrier occupation of the DQDSC structure versus the junction depth x_j, it continues the scenario plotted in Fig. 3. The WL occupations are the smallest in both CB and VB which means that WL works like a reservoir. All the occupations are exponentially declining with junction depth and VB occupations are ~ of the same value while CB occupations are saturated near ~$1\mu m$ junction depth. The occupation of states $\vert 0 \rangle$ and $\vert 1 \rangle$ are raising. This figure confirms both carrier scenarios and the importance of adding the intermediate band (QD layer). The carriers are relaxed from the barrier to WL, and then to the QD states.

Fig. 5 shows the variation of band-to-band recombination rates versus the junction depth. It is shown that the band-to-band recombination rates are similar between right and left QDs where the recombination rate between QD CB GS, $\vert 0 \rangle$, with other two VB QD states $\vert 2 \rangle$ and $\vert 3 \rangle$, i.e. U_{02}, U_{03} and also U_{12}, U_{13} are the same. It also shows that these recombinations are high for nearest states like U_{02}. The WL band-to-band recombination rate U_{45} is very small. This of course explains the reason for using the intermediate band (QD layer) in solar cells.

Fig. 6 shows the relaxation rates between states. The VB recombination rates are R_{57}, R_{35}, R_{23} while those of CB are R_{46}, R_{41}, R_{10}. The VB rates are of the same order and lower than the corresponding CB rates. All rates are raised with occupation except R_{41}, this may be related to its lowest occupation of ρ_{44} compared to other CB occupations as shown in Figs. 3 and 4.

Journal of Education for Pure Science- University of Thi-Qar
Vol.10, No.1 (March., 2020)
Website: jceps.utq.edu.iq   *Email: jceps@eps.utq.edu.iq*

b-Excitonic model at Fermi equilibrium:
Fig. 7 shows the time series in the excitonic model where the occupations are similar to the eh model for CB while there is a difference in the VB occupations due to the change of the initial conditions as a result of including of the Fermi distribution so, the VB in the barrier is assumed to be zero.
Fig. 8 shows the occupations in the excitonic model. Except for the case of the VB barrier, all occupations are not much different from the eh model.
Fig. 9 shows the relaxation rates for the excitonic model. The overall behavior is the same as the eh model. A few increments in the excitonic model in the CB relaxation and VB barrier-WL while a reduction in the VB WL-QD and QD-QD R_{35} and R_{23} rates appear.
Fig. 10 shows the band-to-band recombination rates in the excitonic model. Compared to eh model, while both barrier and WL rates are increased the QD rates U_{02}, U_{13} are reduced.
Fig. 11 shows photo-generation rates for the barrier, WL, and QDs at p- and n-regions. The highest rate is at QD n-region. The lowest WL contribution can be related to their low occupation as in Fig. 9 compared with barrier and QD layers as it works like a reservoir.

7-2Quantum efficiency:
a-e-h model Fermi:
Fig. 12 shows the quantum efficiency (QE) versus the relaxation rates in the eh model. The QE is increased at semi-linear relation with VB relaxation rates while it is increased exponentially with CB rates. The similarity between all VB curves is obvious which comes from the similar relaxation times used for their transitions. QE is reduced only with the R_{41} and R_{40} rate due to the small WL occupation compared with barrier and QD as in Figs. 3 and 4. One must refer that QE appears, at $R_{40} < R_{41}$ which refers to longer recombination time for R_{40} i.e. the longer recombination time for interdot transitions is attained under wider energy difference.
Fig. 13 shows QE versus band-to-band recombination rate in the eh model. Except for WL band-to-band rate U_{45}, QE appears at high rates for both barrier and QDs while it appears at smaller rates for WL due to its smaller occupation as it works like a reservoir. It is shown that the highest band-band rate is U_{13} while the shortest time is U_{02}, i.e. the widest energy difference gives longer band-to-band recombination time. From DQD structure it is shown that longer relaxations and recombinations are confirmed depending on the wider energy difference.

b-excitonic model:
Fig. 14 shows the QE versus the relaxations under the excitonic model. It shows that the lowest relaxation needed for QE is the R_{41}, also the QE is reduced with it is contrary to the effect of other relaxations on QE.
Fig. 15 shows QE versus band-to-band recombination rates. In all the figures, QE is increased with these rates.

8.Conclusions:
This work proposes the DQDSC structure for developing SC properties. The density matrix dynamical equations coupled with the continuity-current equation are solved numerically to obtain QE. For this modeling, the momentum matrix elements of QD-QD, WL-QD, and WL-barrier transitions are considered with the orthogonalized plane wave for WL-QD transitions. Results are simulated both the excitonic and eh cases.
DQD structure is used here for more flexibility in choosing the transition with a long relaxation to attain the best SC properties. These results confirm both the importance of adding the intermediate band (QD

layer) and the carrier scenarios. The band-to-band recombination rates in the DQD structure are modulated with the energy difference. The VB relaxation rates between states are of the same order and lower than the corresponding CB rates related to their occupation. The occupations in the excitonic model do not much differ from the eh model. A few increments in the excitonic model in the CB and VB barrier-WL relaxation while a reduction in the VB WL-QD and QD-QD relaxation appears. The band-to-band recombination rates in the excitonic model are reduced compared to the eh model. The photo-generation rates have the highest rate at QDs. The quantum efficiency (QE) in the eh model is increased at semi-linear relation with VB relaxation rates while it is increased exponentially with CB rates. Longer relaxation times for WL-QD interdot transitions are attained with a wider energy difference. For the DQD structure, the longer relaxations and band-to-band recombinations are confirmed depending on the wider energy difference.

References:

yu, J. Kim, J. Jang, "CdSe quantum dot cathode buffer for inverted organic bulk hetero-junction solar cells", Organic Electronics 13 (2012) 1302–1307.

[2] C. Lin, M. Tan, C. Tsai, K. Y. Chuang, T. S. Lay, "Numerical Study of Quantum-Dot-Embedded Solar Cells", IEEE J. Selected Topics in Quantum Electronics 19 (2013) 4000110.

[3] S. A. Mintairov, N. A. Kalyuzhnyy, M. V. Maximov, A. M. Nadtochiy, S. Rouvimov, and A. E. Zhukov, "GaAs quantum well-dots solar cells with spectral response extended to 1100 nm", Electronics Letters 51 (2015) 1602-1604.

[4] A. Luque, A. Panchak, I. Ramiro, P. Garcia-Linares, A. Mellor, E. Antolın, A. Vlasov, V. Andreev, and A. Marti, "Quantum Dot Parameters Determination from Quantum-Efficiency Measurements", IEEE J. Photovoltaics 5 (2015) 1074-1078.

[5] D. Kim, M. Tang, J. Wu, S. Hatch, Y. Maidaniuk, V. Dorgan, Y. I. Mazur, G. J. Salamo, and H. Liu, "Si-doped InAs/GaAs Quantum-Dot Solar Cell with AlAs Cap Layers", IEEE J. Photovoltaics 6 (2016) 906-911.

[6] D. Kim, S. Hatch, J. Wu, K. A. Sablon, P. Lam, P. Jurczak, M. Tang, W. P. Gillin, and H. Liu, "Type-II InAs/GaAsSb Quantum Dot Solar Cells with GaAs Interlayer", IEEE J. Photovoltaics 8 (2018) 741-745.

[7] I. Ramiro, J. Villa, P. Lam, S. Hatch, J. Wu, E. Lopez, E. Antolin, H. Liu, A. Martı, and A. Luque, "Wide-Bandgap InAs/InGaP Quantum-Dot Intermediate Band Solar Cells", IEEE J. Photovoltaics 5 (2015) 840-845.

[8] D. Kim, S. Hatch, J. Wu, K. A. Sablon, P. Lam, P. Jurczak, M. Tang, W. P. Gillin, and H. Liu, "Type-II InAs/GaAsSb Quantum Dot Solar Cells with GaAs Interlayer", IEEE J. Photovoltaics 8 (2018) 741-745.

[9] M. Gioannini, A. Cedola, F. Cappelluti, "Impact of carrier dynamics on the photovoltaic performance of quantum dot solar cells", IET Optoelectronics 9, (2015) 69-74.

[10] M. Gioannini and Ariel P. Cedola, "Simulation of Quantum Dot Solar Cells Including Carrier Intersubband Dynamics and Transport", IEEE J. Photovoltaics 3, 1271-1278 (2013).

[11] "A. Cedola, F. Cappelluti and M. Gioannini, "Dependence of quantum dot photocurrent on the carrier escape nature in InAs/GaAs quantum dot solar cells", Semicond. Sci. Technol. 31, 025018 (2016).

[12] F. Cappellutin, M. Gioannini, A. Khalili, "Impact of doping on InAs/GaAs quantum-dot solar cells: A numerical study on photovoltaic and photoluminescence behavior", Solar Energy Materials & Solar Cells 157, 209–220 (2016).

[13] J. M. Villas-Bôas, A. O. Govorov, and S. E. Ulloa, "Coherent control of tunneling in a quantum dot molecule", Phys. Rev. B 69 (2004) 125342.

[14] H. S. Borges, L. Sanz, J. M. Villas-Boas, O. D. Neto, and A. M. Alcalde, "Tunneling induced transparency and slow light in quantum dot molecules," Phys. Rev. B 85 (2012) 115425.

[15] B. Al-Nashy, S. M. M. Amin and Amin H. Al-Khursan, "Kerr effect in Y- configuration double quantum dot System", J. Opt. Soc. Am. B 31 (2014) 1991-1996.

[16] M. Abdullah, Farah T. Mohammed Noori, and Amin H. Al-Khurasan, "Terahertz emission in ladder plus Y-configurations in double quantum dot structure", Applied Optics 16 (2015) 5186-5192.

[17] F. R. Al-Salihi and Amin Habbeb Al-Khursan, "Electromagnetically induced grating in double quantum dot system", Optical and Quantum Electronics 52 (2020) 185.

[18] F. K. Hachim, F. H. Hannon, and Amin Habbeb Al-Khursan, "Adaptive prism using double quantum dot structure" Applied Optics 59 (2020) 2759-2766.

[19] L. Seravalli, M. Gioannini, F. Cappelluti, F. Sacconi, G. Trevisi, and P. Frigeri, "Broadband light sources based on InAs/InGaAs metamorphic quantum dots", J. Appl. Phys. 119 (2016) 143102.

[20] S. N. Dwara and Amin H. Al-Khursan, "Quantum Efficiency of InSbBi Quantum Dot photodetector", Applied Optics 54, 9722-9727 (2015).

[21] S. N. Dwara and A. H. Al-Khursan, "Two-window InSbBi quantum-dot photodetector", Applied Optics 55, 5591-5595 (2016).

[22] M. Gioannini and I. Montrosset, "Numerical Analysis of the Frequency Chirp in Quantum-Dot Semiconductor Lasers", IEEE Quantum electronics 43 (2007) 941-494.

[23] Y. Ben Ezra, B. I. Lembrikov, and M. Haridim, "Specific features of XGM in QD-SOA," IEEE J. Quantum Electron. 43, 730–737 (2007).

[24] A. H. Flayyih and A. H. Al-Khursan, "Integral gain in quantum dot semiconductor optical amplifiers", Superlattices Microstruct. 62, 81–87 (2013).

Tables:

Table1: Parameters of DQDSC structure [12, 13].

Parameter	Symbol	Value
Diffusion length of n-doped layer (m)	L_n	0.1×10^{-6}
Diffusion length of p-doped layer (m)	L_p	0.25×10^{-6}
Depletion region width (m)	W	0.48×10^{-6}
Layer thickness (m)	H	1.6×10^{-6}
Reflectivity	R	0.99
Photon flux	Φ	10^8
Hole lifetime (s)	τ_p	0.054×10^{-9}
Electron lifetime (s)	τ_n	0.54×10^{-9}
Surface recombination velocity in the p-layer	S_p	0
Surface recombination velocity in the n-layer	S_n	0

Table 2: Calculated linear absorption (m^{-1}) **in the layers:**

Parameter	Symbol	Value
n-doped QD layer	α_n	3×10^6
p-doped QD layer	α_p	5×10^6
QDs in depletion-region	α_d	2.3×10^6
n-doped wL	α_{nw}	3×10^3
p-doped wL	α_{pw}	4×10^3
n-doped Barrier region	α_{nB}	3×10^2
p-doped Barrier region	α_{pB}	5×10^2

Table 3: Relaxation times of the DQDSC system [4, 15].

Parameter (unit)	Value	Parameter (unit)	Value
$\tau_{o_{40}}(s)$	1×10^{-12}	$\tau_{o_{04}}(s)$	1×10^{-9}
$\tau_{o_{41}}(s)$	3×10^{-12}	$\tau_{o_{14}}(s)$	1×10^{-9}
$\tau_{o_{10}}(s)$	0.1×10^{-12}	$\tau_{o_{01}}(s)$	1.2×10^{-12}
$\tau_{o_{64}}(s)$	0.3×10^{-12}	$\tau_{o_{46}}(s)$	0.3×10^{-12}
$\tau_{o_{32}}(s)$	0.1×10^{-12}	$\tau_{o_{23}}(s)$	0.1×10^{-12}
$\tau_{o_{25}}(s)$	0.1×10^{-12}	$\tau_{o_{52}}(s)$	0.1×10^{-12}
$\tau_{o_{35}}(s)$	0.1×10^{-12}	$\tau_{o_{53}}(s)$	0.1×10^{-12}
$\tau_{o_{75}}(s)$	0.1×10^{-12}	$\tau_{o_{57}}(s)$	0.1×10^{-12}
$\tau_{o_{20}}(s)$	2.8×10^{-9}	$\tau_{o_{31}}(s)$	2.8×10^{-9}
$\tau_{o_{30}}(s)$	2.8×10^{-9}	$\tau_{o_{45}}(s)$	10×10^{-9}
$\tau_{o_{21}}(s)$	2.8×10^{-9}	$\tau_{o_{67}}(s)$	100×10^{-9}

Figures:
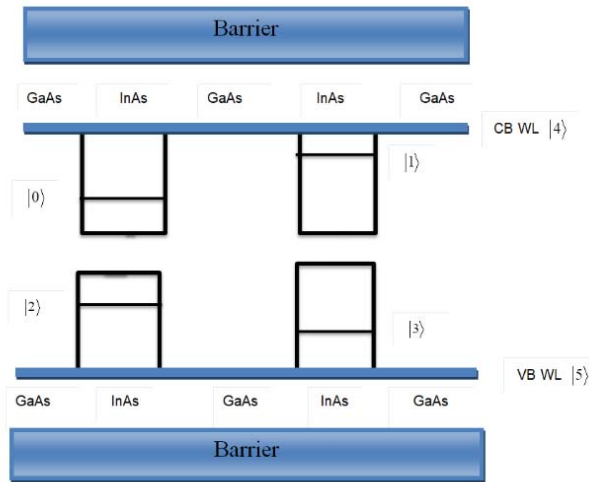
Fig. 1: DQD structure that is used in the solar cell.
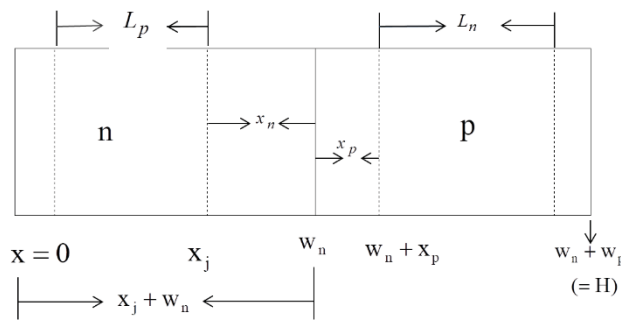
Fig. 2: A schematic representation of the structure of the layers of QD solar cells.
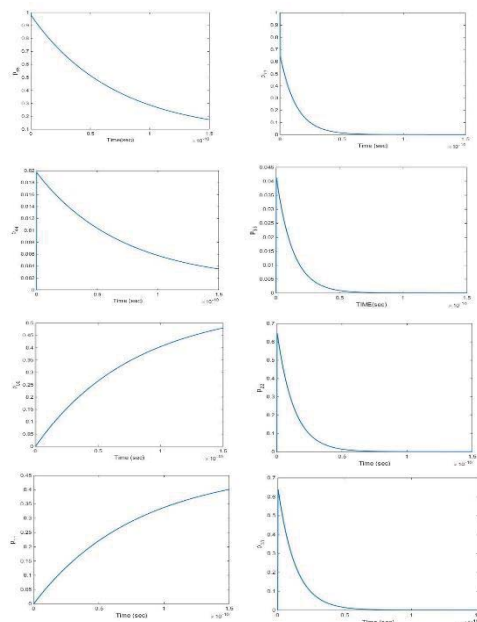
Fig. 3: Time series of DQDSC states in the eh model assuming Fermi distribution.
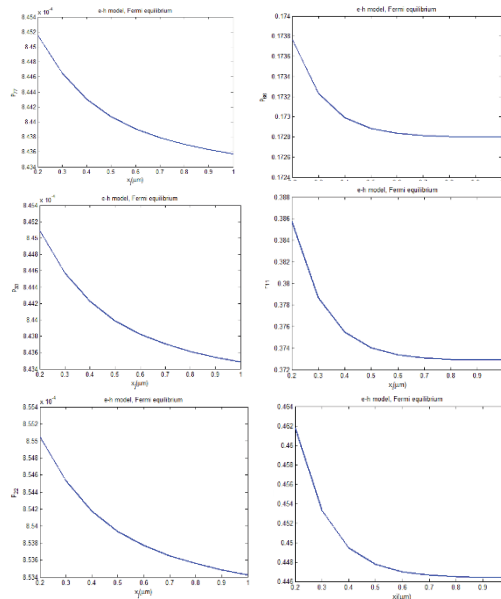
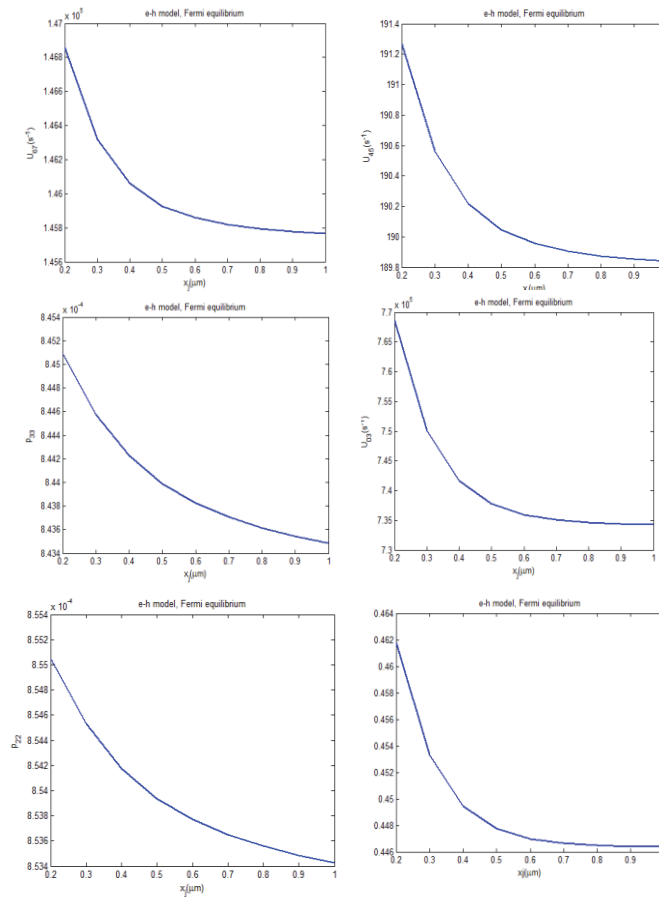**Fig. 4: DQDSC carrier occupation versus the junction depth** x_j .

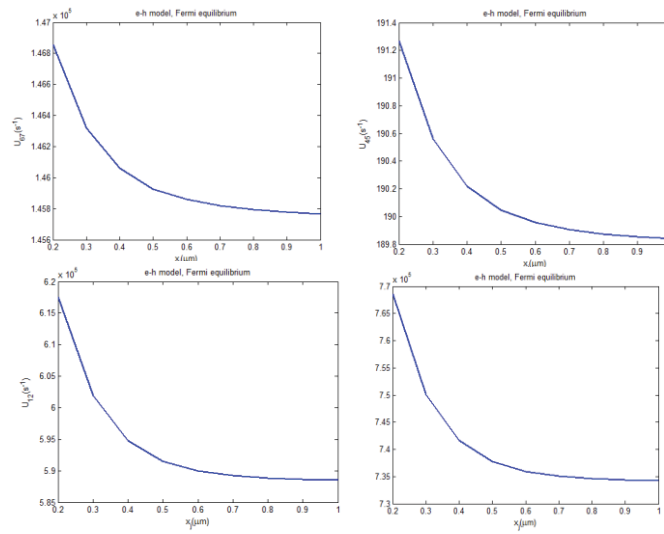**Fig. 4: DQDSC carrier occupation versus the junction depth** x_j .

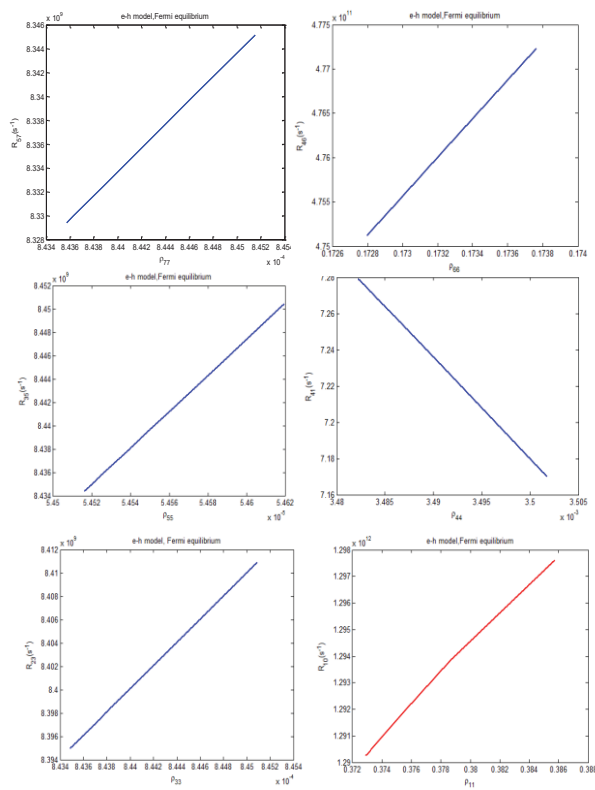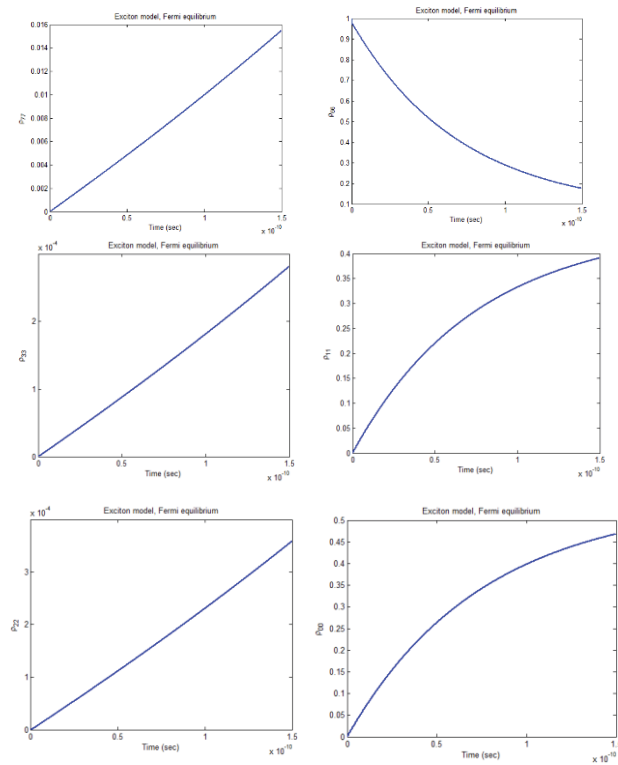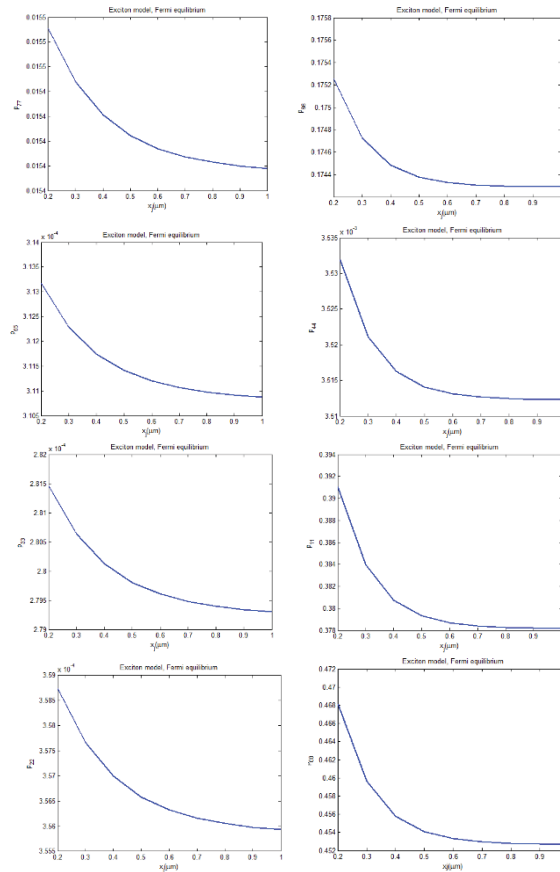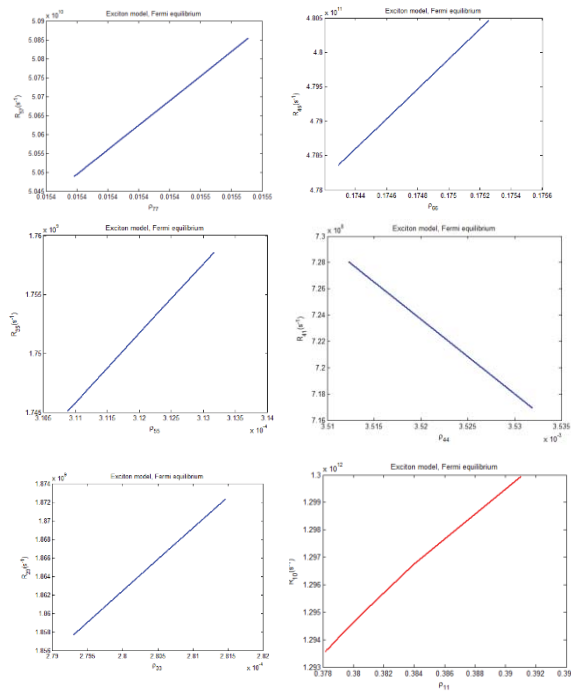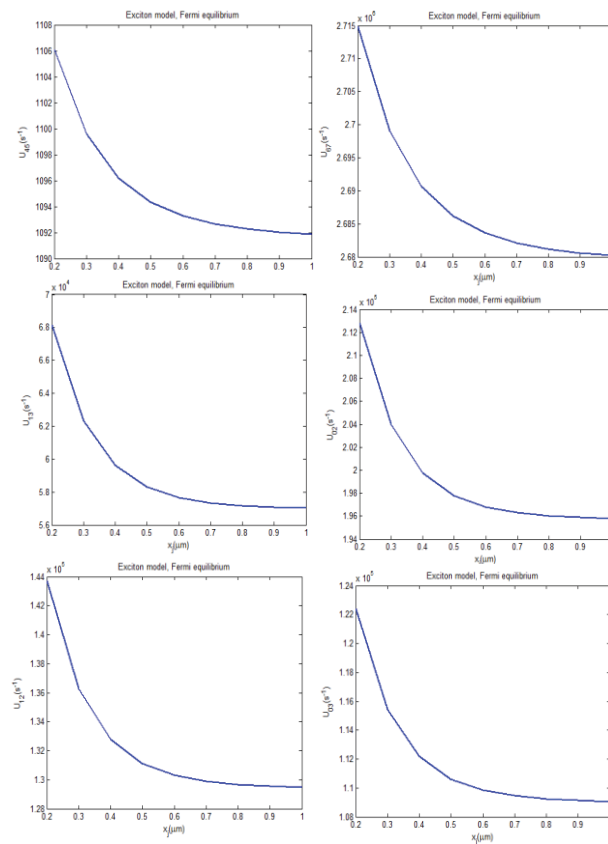**Fig. 5: DQDSC band-to-band recombination rates versus carrier occupation.**

Fig. 6: DQDSC the relaxation rates between states versus the carrier occupation.

Fig. 7: Time series of DQDSC states in the excitonic model assuming Fermi distribution.

Fig. 8: DQDSC carrier occupation versus the junction depth x_j .

Journal of Education for Pure Science- University of Thi-Qar
Vol.10, No.1 (March., 2020)
Website: jceps.utq.edu.iq   *Email: jceps@eps.utq.edu.iq*

Fig. 9: DQDSC carrier relaxation rates versus the junction depth x_j .

Fig. 10: DQDSC band-to-band recombination rates versus the junction depth x_j .
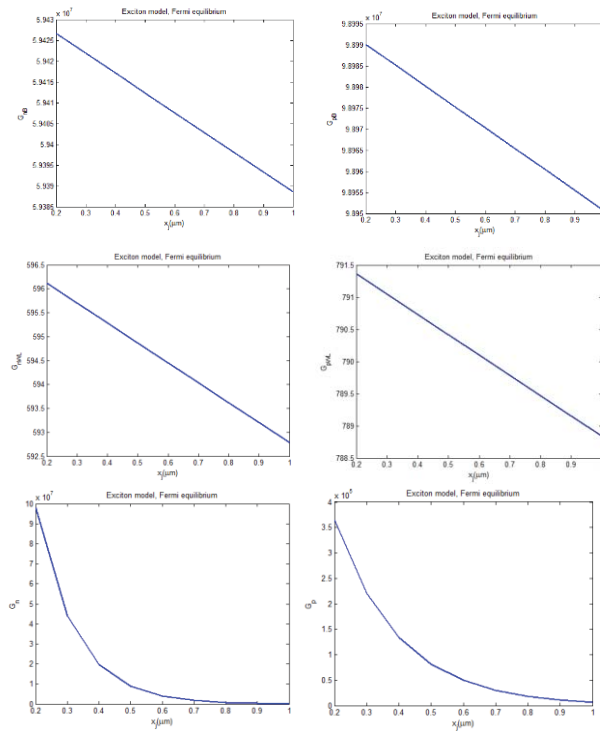
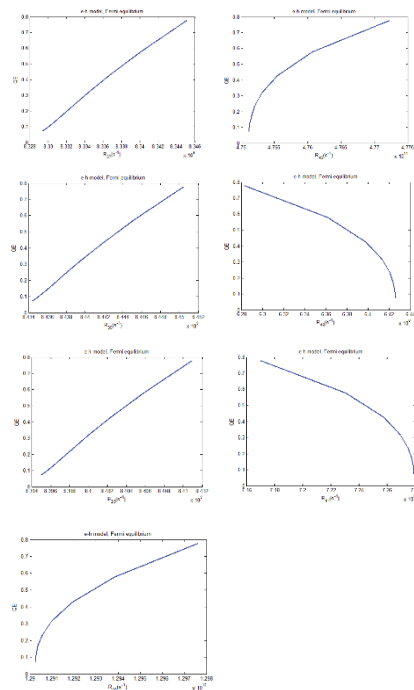**Fig. 11: DQDSC photo-generation recombination rates versus the junction depth x_j .**

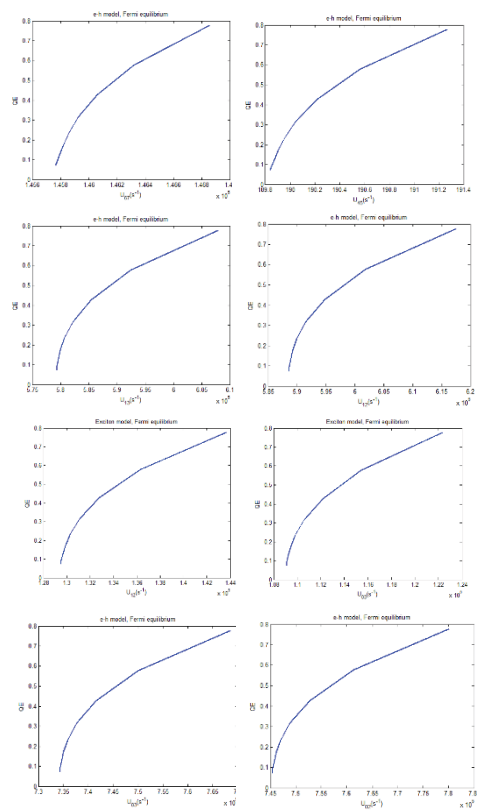
Fig. 12: QE versus the relaxation rates between states.

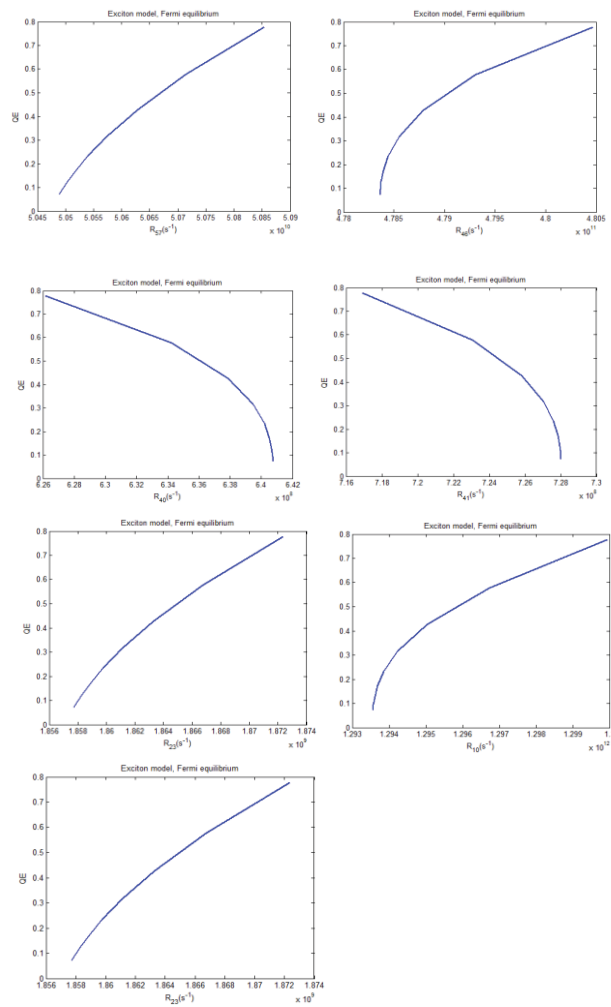**Fig. 13: The QE versus band-to-band recombination rates.**

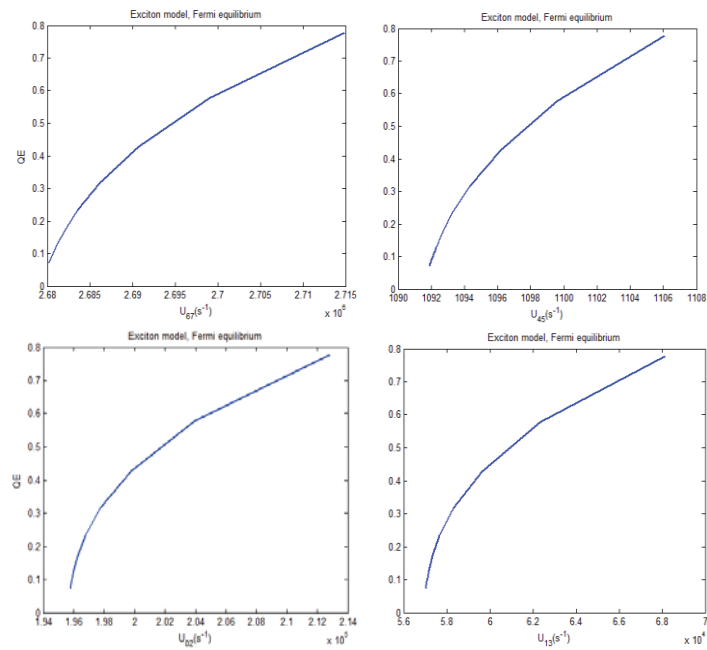**Fig. 14:** **DQDSC relaxation rates versus the junction depth** x_j **.**

Fig. 15: **DQDSC relaxation rates versus the junction depth** x_j **.**